14th World Congress in Computational Mechanics (WCCM)
ECCOMAS Congress 2020
Virtual Congress: 11 – 15 January 2021
F. Chinesta, R. Abgrall, O. Allix and M. Kaliske (Eds)

TOTAL FOCUSING METHOD FOR IMAGING DEFECT IN CFRP COMPOSITE WITH ANISOTROPY AND INHOMOGENEITY

HAI XIAO[1], MENGLONG LIU[1], SHIFENG GUO[2] AND FANGSEN CUI[3]

[1] School of Mechanical Engineering and Automation, Harbin Institute of Technology, Shenzhen 518055, P.R. China
liumenglong@hit.edu.cn

[2] Shenzhen Key Laboratory of Smart Sensing and Intelligent Systems, Shenzhen Institutes of Advanced Technology, Chinese Academy of Sciences, Shenzhen 518055, P.R. China
sf.guo@siat.ac.cn

[3] Institute of High Performance Computing, A*STAR (Agency for Science, Technology and Research), 138632, Singapore
cuifs@ihpc.a-star.edu.sg

Keywords: Fiber reinforced polymer, Dynamic homogenization, Floquet wave, Total focusing method

Abstract. Fiber reinforced polymers (FRPs) are increasingly used in thick primary load-bearing structures, while manufacturing and in-service defects occur with a higher chance as the composite thickness increases, which entails the nondestructive detection and evaluation of potential structure defects. This study focuses on the imaging qualities of defects at different depth in thick FRPs via total focusing method (TFM), aiming at determining the optimum imaging strategy for thick FRPs (25 mm for discussion). Dynamic homogenization based on Floquet theory and numerical finite element analysis are performed to interrogate the wave propagation characteristics. The Frequency-dependent time correction method for TFM imaging (F-TFM) is proposed for accurate defect imaging in periodically layered crossply FRP. Finally, the results show that the proposed F-TFM method is able to detect and locate the defects of 2 mm size at all possible depth.

1. INTRODUCTION

Fiber reinforced polymer composites are promising materials for almost every industry looking for low weight and high strength materials. They have been widely used in aerospace, automotive, marine and even highly sensitive biomedical industry[1–3]. Compared with conventional metal materials, FRPs have the advantages of light weight, high specific strength, high corrosion resistance, excellent fatigue durability, high designability and large-scale integral molding[4].

FRPs have increasingly been used in primary and secondary load-bearing thick structures where a mechanical failure has much greater safety concern. Due to the special multi-layer

structure and different manufacturing methods from traditional metallic material, there are more defects and damage forms in FRP composites apart from those that metallic materials might have. Manufacturing defects in FRP composites include unevenly distributed or bunched fibers, in-plain fiber waviness, out-of-plain fiber wrinkling, voids which arise from poor resin infusion, missing piles or incorrect ply orientation due to human error, and localized crushing and fracture that might promote delamination due to additional drilling and fastening steps[5]. In-service defects, such as matrix cracking, delamination and adhesive disbonding, fiber fracture and other barely-visible damages caused by surface impacts, often occur inside the complex structures and cannot be visually inspected. Therefore, to inspect and characterize composite structures using nondestructive testing and evaluation (NDT&E) method is quite necessary.

Among all the NDT&E techniques for FRP composite, ultrasonic testing (UT) is the most widely used one for its online testing capability of internal defects with relatively low cost and great convenience[6,7]. The multi-channel-based UT approach, which features a combination of signal feature from multiple signal sources, overcomes limitations of low energy and depth focuses when adopting pulse-echo or through-transmission method. Among multi-channel-based methods, TFM has the highest signal-to-noise ratio and has been increasingly used in defects detection[8,9]. For anisotropic materials, a time-correction-based wave velocity anisotropy is necessary. Li et al.[10] measured the wave velocity on quasi-isotropic FRP composites experimentally and obtained imaging results of SDH with 2 MHz central frequency showing the best imaging quality. Luo et al.[11] selected the 5 MHz central frequency to image the artificial delamination in FRP, obtaining a fairly good imaging. These researches validated the feasibility of time-corrected TFM for FRP, but lack a systematic analysis on how the excitation central frequency influence the TFM imaging quality of the defects at different depth.

To obtain an accurate TFM imaging of thick FRP laminate, this study is dedicated to the fundamental interrogation of wave propagation characteristics in FRP via Floquet wave theory and numerical finite element analysis (FEA). A dynamic homogenization for inhomogeneous and anisotropic FRP laminate is performed to discover the wave propagation characteristics. Finite element modeling of wave propagation in FRP is followed. Finally, a frequency-dependent time-corrected TFM (F-TFM) defect imaging technique is proposed for thick FRP laminate.

The rest of the paper is organized as follows. Section 2 and section 3 describe the analytical formulation and numerical modeling of wave propagation in FRP respectively. Based on both analytical and numerical analyses, the F-TFM imaging for FRP laminate is proposed in Section 4, to optimize the defect imaging quality. Lastly, concluding remarks are presented in Section 5.

2. ANALYRICAL FORMULATION

2.1 Floquet wave homogenization

According to the Christoffel equation, no wave velocity dispersion effect needs to be considered for homogeneous material. Nevertheless, for periodically layered FRP, the different ply stack-up orientation makes the entire structure inhomogeneous, resulting in wave reflections and refractions at the interfaces. Floquet homogenization assumes that the inhomogeneous periodic structure can be homogenized as a homogeneous one in terms of wave propagation at a specific frequency and propagation direction range. In this way, only a

minimum periodic cell unit needs to be modelled to interrogate the wave propagation in thick periodically layered FRP.

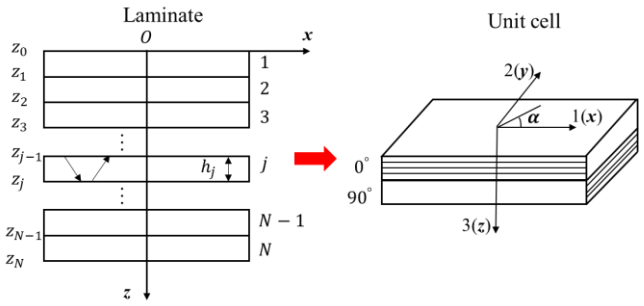

Figure 1: A multilayered structure and coordinate system.

The wave propagation characteristic in a periodic cell unit is derived based on the Floquet wave theory and recursive stiffness matrix method[12]. The waves propagating in periodically layered FRP are referred as Floquet waves. The characteristic equation for the Floquet wave is given by

$$\det(e^{i\beta d}\mathbf{K}_{21}^{c} - e^{-i\beta d}\mathbf{K}_{12}^{c} + \mathbf{K}_{22}^{c} - \mathbf{K}_{11}^{c}) = 0\,, \tag{1}$$

where $\mathbf{K}_{ij}^{c}$ denotes the four submatrices of the total stiffness matrix, β is the Floquet wavenumber and d is the thickness of the laminate. In the interval $-\pi < \beta d < \pi$, six solutions can be obtained, among which complex ones represent evanescent waves and real ones are propagating waves. These two kinds of wave are described by stop and pass bands of the Floquet wave spectrum.

2.2 Dynamic homogenization regions

Supposing a wave incident from water to the investigated $[0/90]_{100}$ FRP laminate of ply thickness 125 um in the $x-z$ plane, with the lamina property listed in **Table 1**, the pass and stop bands of the unit cell [0/90] in the incidence angle and frequency domains are displayed in **Figure 2**. The number of Floquet waves is restricted to be two as no motion in y direction will be generated.

Table 1: Properties of one lamina.

Elastic constants of one lamina (GPa)	
C_{11}	143.2
C_{22}	15.8
C_{12}	7.5
C_{23}	8.2
C_{55}	7.0
Density (kg/m^3)	1600
Thickness (mm)	0.125

The regions in **Figure 2** can be classified as concluded below:

(1) Fully homogeneous region. There are two propagating waves in this fully

homogeneous region and FRP can be considered as a fully homogeneous medium in terms of wave propagation.

(2) Partially homogeneous region. Region in gray occupies most of the analysis domain, wherein one propagating and one evanescent wave exist.

(3) Inhomogeneous region. In regions with black color, there is no propagating wave.

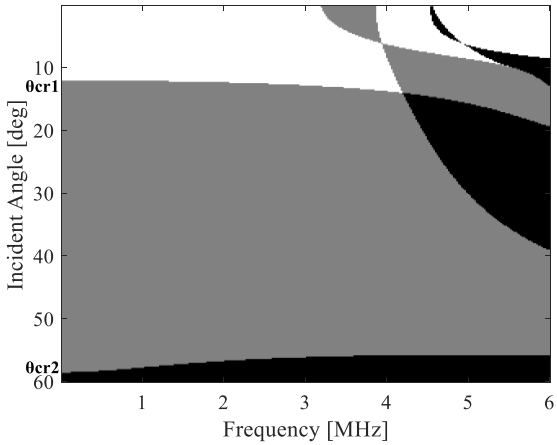

Figure 2: Bands of the Floquet waves for cross-ply unit cell ([0/90]) (white: pass band, two propagating waves; gray: one propagating wave; black: stop band, no propagating wave)

3. NUMERICAL MODELING

3.1 FEM setup

To further explore the wave propagation characteristics in multidirectional FRP, intact laminates models are built via the finite element platform OnScale® as illustrated in **Figure 3**. A plane strain FRP model with $x - z$ dimensions of 118.1 mm × 25 mm is built, which is with stack-up orientation of $[0/90]_{100}$ with 125 um ply thickness. The mesh size is 0.025 mm and 0.04 mm in the x and z directions, respectively, which has been testified to accurately model the wave propagation at mentioned pulse frequencies 1 ~ 4 MHz.

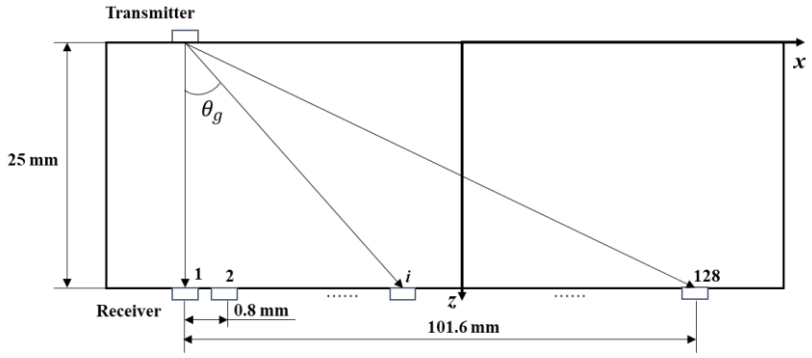

Figure 3: Intact laminate model for thru-transmission test.

The excitation signal which simulates the emission of ultrasonic waves is a normalized Ricker wavelet. Absorbing boundary conditions and free boundary conditions are applied to the

left-right and top-bottom geometry boundaries, respectively. By activating element 1 as a transmitter, the receiving signals through receivers 1-128 with center-to-center space being 0.8 mm in the bottom are captured by averaging the time history of acoustic pressure over each receiver element. In this way, the group velocities along 128 directions are calculated by dividing the distance from transmitter to receiver i ($i = 1,..,128$) by the travel time to corresponding element.

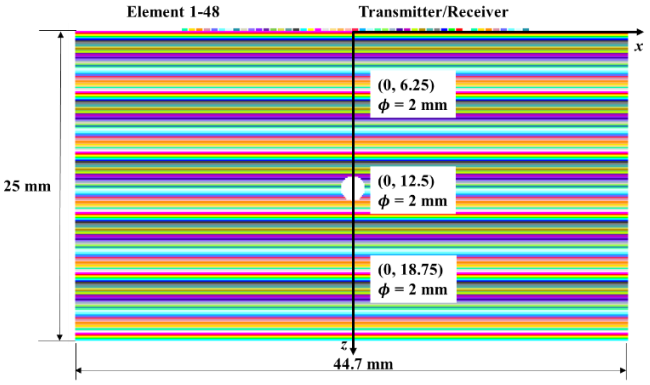

Figure 4: FEA model of FRP laminates with an SDH.

Finite element models of wave propagation in crossply FRPs of 25 mm thick in total and 125 um thick ply with side-drilled holes (SDHs) are also built. The FRP setups are almost the same as the intact ones. The difference is that an SDH of diameter $\phi = 2$ mm located 6.25/12.5/18.75 mm deep from the surface is built to simulate the defect in the specimen. On the top surface of the model, 48 rectangles of 0.5 mm length and 0.6 mm pitch are considered as ultrasonic array elements, ranging from $x_1 = -14.1$ mm to $x_{48} = -14.1$ mm. By exciting each element in turn and acquiring the time history of average acoustic pressure, a 48×48 full matrix capture (FMC) dataset of response signals is obtained.

3.2 Result analysis

Group velocity profiles of crossply FRP shown in **Figure 3** are compared via analytical modeling and numerical modeling, with results displayed in **Figure 5**. A comparison is performed for the crossply FRP at 2 MHz and 4 MHz. It is observed that the group velocity obtained through both analytical and numerical modeling are well corroborated, giving a statistical average error less than 1%. In addition, just as the analytical model indicates, the crossply structure indeed generates a frequency-related wave dispersion in the FEA model, that a higher frequency corresponds to a lower group velocity at the same group velocity refraction angle.

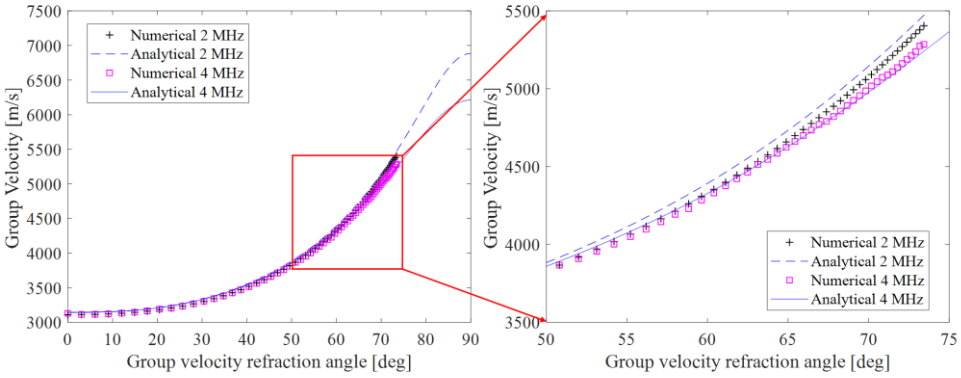

Figure 5: Comparison of analytical and numerical modeling results of group velocities in crossply FRP (125 um ply thickness) at $f_c = 2$ MHz and 4 MHz.

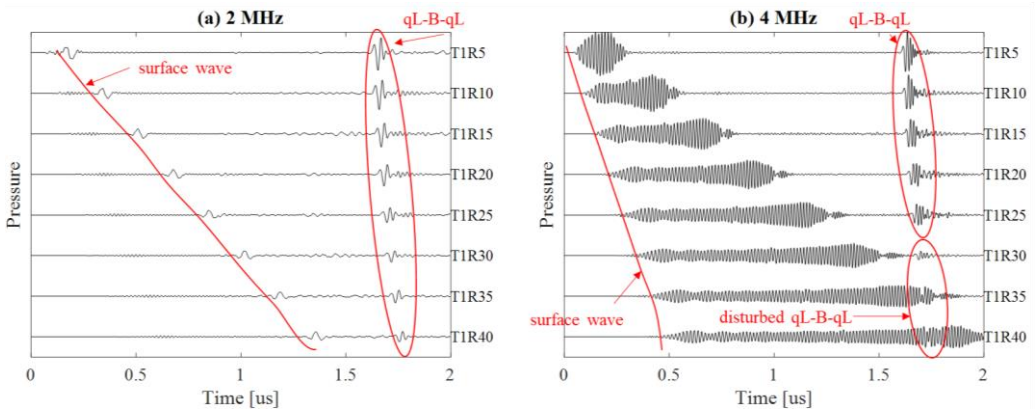

Figure 6: Time domain signals in crossply FRP $[0/90]_{100}$ (125 um ply thickness), element 1 as transmitter. (a) $f_c = 2$ MHz, (b) $f_c = 4$ MHz.

The time domain signals obtained via simulation based on model shown in **Figure 4** when the depth of SDH is 12.5 mm at 2 MHz and 4 MHz are given as **Figure 6**. It is observed that the prominent components of received signals are surfaces wave and the reflected qL from the backwall (qL-B-qL). The arrival time of surface waves increases as the distance from receiver to transmitter increases. Nevertheless, the travel times of the qL-B-qL are almost the same, which is attributed to the combined effect of increased travel distance and increased group velocity at higher refraction angle. The arrival time of the fastest wave scattered from SDH (qL-S-qL) wave can be easily distinguished at 2 MHz, while at 4 MHz the received signals are totally distorted and elongated, which may be due to the interply wave reflection and refraction and hence no SDH scattered wave can be observed.

4. FREQUENCY-DEPENDENT TIME-CORRECTED TFM (F-TFM)

4.1 Methodology

Following a detailed interrogation of Floquet wave in periodic layered FRP via analytical and numerical methods, the F-TFM developed from the conventional TFM, is proposed in this study to optimize the defect imaging in FRP. For any image point (x, z), the pixel value is given

by

$$I(x,z) = \left| \sum_{i=1}^{n} \sum_{j=1}^{n} h_{ij}(t_i(x,z) + t_j(x,z)) \right| \tag{2}$$

where h_{ij} is the time-history record of element j located at position x_j when element i located at position x_i is activated as a transmitter. The time delays $t_i(x,z)$ and $t_j(x,z)$ are the wave travel time from element i and element j to image point (x,z) respectively, which are obtained by dividing the distances by velocities of the fastest Floquet wave in corresponding propagation direction. As indicated in the phase/group velocity profile of crossply FRP displayed in **Figure 5**, the wave propagation velocity anisotropy characteristic is strongly dependent on wave frequency, the proposed F-TFM adopts the frequency-dependent group velocity correction. In this way, the energy focusing can be achieved with highest accuracy.

4.2 TFM imaging

The normalized imaging results of FEM models with one SDH at 6.25/12.5/18.75 mm depth via the proposed F-TFM are displayed in **Figure 7**. It is observed that lower frequencies correspond to a clearer imaging quality, while at the higher frequencies the imaging results do not show the defects clearly.

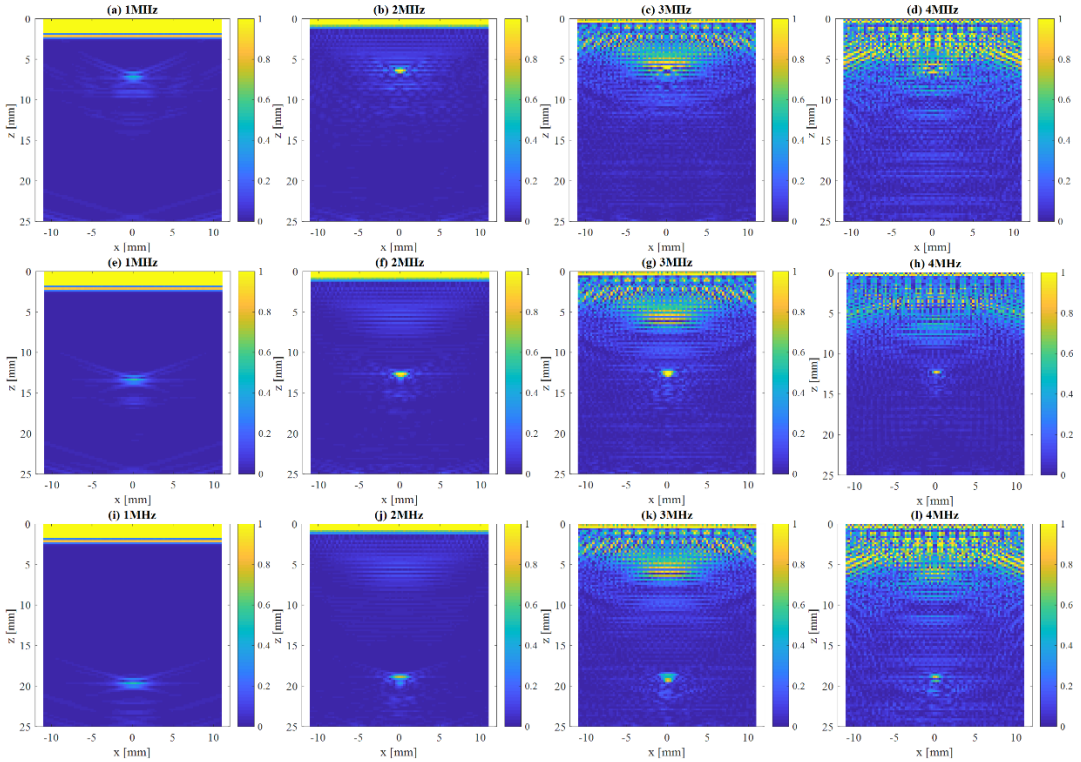

Figure 7: F-TFM imaging results of crossply FRP $[0/90]_{100}$. (a-d): $z_{SDH} = 6.25$ mm, (e-h): $z_{SDH} = 12.5$ mm, (e-h): $z_{SDH} = 18.75$ mm. (a, c, i): $f_c = 1$ MHz, (b, f, j): $f_c = 2$ MHz, (e, g, k): $f_c = 3$ MHz, (d, h, l): $f_c = 4$ MHz.

For relatively shallower preset SDH in the FEM model, its imaging quality is more likely to be influenced by the near-field effect at higher frequencies, which is attributed to the interply

wave reflection and refraction. **Figure 7**(e, d) show that at 3 ~ 4 MHz, the SDH cannot be detected, as the SDHs are blurred by the near-field effect. Images at lower excitation frequencies show better resolution regardless of the depth of SDH, especially at 2 MHz. The deeper defects are more likely to be detected as they are immune to the so-called near-field effect and hence generate images with better quality.

Therefore, the selection of optimum excitation frequency for the proposed F-TFM depends on the depth of the defects. For shallower defects, low frequencies may contribute to a better image quality (1 ~ 2MHz), while for deeper defects relatively higher excitation frequencies (2 ~ 3 MHz) may help with the energy focusing because waves with higher frequencies have a smaller wavelength, although they may cause much severer interply refraction and reflection in the near field. In this case with 25 mm thick FRP, 2 MHz is the optimum selection to detect possible defects at all depth.

5. CONCLUDING REMARKS

In this study, the F-TFM for defect imaging at different depth is proposed for thick periodically layered FRP with high accuracy. By adopting Floquet wave theory to achieve dynamic homogenization and finite element analysis, the wave propagation characteristics at multilayered FRPs are intensively interrogated. It is observed that the at different wave frequencies, the periodic FRP structure makes the propagating wave dispersive, thus a time-correction tailored to each specific frequency is proposed to focus the wave energy. By comparing image quality via the proposed F-TFM with 2 mm SDH preset at different depth, it is concluded that the optimum excitation frequency to detect defects in a $[0/90]_{100}$ with 125 um thickness is around 2 MHz, which contradicts to the common sense that a higher frequency usually gives a strong wave scattering from defects and hence gets TFM images with better quality. Waves at higher frequencies may cause severe interply reflection and refraction, which may lead to a distortion to the imaging effect of defects near the contact surface. This study interrogates the wave dispersion phenomenon caused by FRP crossply stack-up, which is another factor to be considered when performing time compensation and will be further discussed in future research.

ACKNOWLEDGEMENT

Menglong Liu would like to thank the support from the Foundation Committee of Fundamental and Applied Fundamental Research of Guangdong Province (Grant No. 2019A1515110704).

REFERENCES

[1] P.K. Bajpai, I. Singh, Reinforced Polymer Composites: Processing, Characterization and Post Life Cycle Assessment, Wiley-VCH Verlag GmbH & Co. KGaA, Weinheim, Germany, 2020. https://doi.org/10.1002/9783527820979.

[2] P.K. Bajpai, F. Ahmad, V. Chaudhary, Processing and characterization of bio-composites, in: Handb. Ecomater., Springer International Publishing, 2019: pp. 123–139. https://doi.org/10.1007/978-3-319-68255-6_98.

[3] R.H. Bossi, G.E. Georgeson, Nondestructive testing of aerospace composites, in: Polym. Compos. Aerosp. Ind., Elsevier, 2020: pp. 461–489. https://doi.org/10.1016/b978-0-08-102679-3.00016-2.

[4] Y. Wang, R. Guan, Y. Lu, Nonlinear Lamb waves for fatigue damage identification in FRP-reinforced steel plates, Ultrasonics. 80 (2017) 87–95. https://doi.org/10.1016/j.ultras.2017.05.004.

[5] M.E. Ibrahim, Nondestructive evaluation of thick-section composites and sandwich structures: A review, Compos. Part A Appl. Sci. Manuf. 64 (2014) 36–48. https://doi.org/10.1016/j.compositesa.2014.04.010.

[6] Z. Zhang, S. Guo, Q. Li, F. Cui, A.A. Malcolm, Z. Su, M. Liu, Ultrasonic detection and characterization of delamination and rich resin in thick composites with waviness, Compos. Sci. Technol. 189 (2020) 108016. https://doi.org/10.1016/j.compscitech.2020.108016.

[7] M. Liu, S. Chen, Z.Z. Wong, K. Yao, F. Cui, In situ disbond detection in adhesive bonded multi-layer metallic joint using time-of-flight variation of guided wave, Ultrasonics. 102 (2020) 106062. https://doi.org/10.1016/j.ultras.2020.106062.

[8] B.W. Drinkwater, P.D. Wilcox, Ultrasonic arrays for non-destructive evaluation: A review, NDT E Int. 39 (2006) 525–541. https://doi.org/10.1016/j.ndteint.2006.03.006.

[9] W. Li, Z. Zhou, Y. Li, Application of Ultrasonic Array Method for the Inspection of TC18 Addictive Manufacturing Titanium Alloy, Sensors. 19 (2019) 4371.

[10] C. Li, D. Pain, P.D. Wilcox, B.W. Drinkwater, Imaging composite material using ultrasonic arrays, NDT E Int. 53 (2013) 8–17. https://doi.org/10.1016/j.ndteint.2012.07.006.

[11] L. Lin, H. Cao, Z. Luo, Total focusing method imaging of multidirectional CFRP laminate with model-based time delay correction, NDT E Int. 97 (2018) 51–58. https://doi.org/10.1016/j.ndteint.2018.03.011.

[12] D. Chimenti, S. Rokhlin, P. Nagy, Physical Ultrasonics of Composites, Oxford University Press, 2011. https://doi.org/10.1093/oso/9780195079609.001.0001.